Published in final edited form as:
Acta Biomater. 2020 August ; 112: 190–201. doi:10.1016/j.actbio.2020.05.008.

Assessing and improving the biocompatibility of microfluidic artificial lungs

Alex J. Thompson[a,b,*], **Lindsay J. Ma**[a,b], **Terry Major**[b], **Mark Jeakle**[b], **Orsolya Lautner-Csorba**[b], **Marcus J. Goudie**[c], **Hitesh Handa**[c], **Alvaro Rojas-Peña**[b], **Joseph A. Potkay**[a,b]

[a]VA Ann Arbor Healthcare System, 2215 Fuller Road, Ann Arbor, MI, USA, 48105

[b]University of Michigan, 1150 W. Medical Center Drive, Ann Arbor, MI, USA, 48109

[c]University of Georgia, College of Engineering, 220 Riverbend Road, Athens, GA, USA, 30602

Abstract

Microfluidic artificial lungs (μALs) have the potential to improve the treatment and quality of life for patients with acute or chronic lung injury. In order to realize the full potential of this technology (including as a destination therapy), the biocompatibility of these devices needs to be improved to produce long-lasting devices that are safe for patient use with minimal or no systemic anticoagulation. Many studies exist which probe coagulation and thrombosis on polydimethyl siloxane (PDMS) surfaces, and many strategies have been explored to improve surface biocompatibility. As the field of μALs is young, there are few studies which investigate biocompatibility of functioning μALs; and even fewer which were performed *in vivo*. Here, we use both *in vitro* and *in vivo* models to investigate two strategies to improve μAL biocompatibility: 1) a hydrophilic surface coating (polyethylene glycol, PEG) to prevent surface fouling, and 2) the addition of nitric oxide (NO) to the sweep gas to inhibit platelet activation locally within the μAL. In this study, we challenge μALs with clottable blood or platelet-rich plasma (PRP) and monitor the resistance to blood flow over time. Device lifetime (the amount of time the μAL remains patent and unobstructed by clot) is used as the primary indicator of biocompatibility. This study is the first study to: 1) investigate the effect of NO release on biocompatibility in a microfluidic network; 2) combine a hydrophilic PEG coating with NO release to improve blood compatibility; and 3) perform extended *in vivo* biocompatibility testing of a μAL. We found that μALs challenged *in vitro* with PRP remained patent significantly longer when the sweep gas contained NO than without NO. In the *in vivo* rabbit model, neither approach alone (PEG coating nor NO sweep gas) significantly improved biocompatibility compared to controls (though with larger sample size significance may become apparent); while the combination of a PEG coating with NO sweep gas resulted in significant improvement of device lifetime.

[*]Corresponding Author. ajthomp@umich.edu (A.J. Thompson).

Declaration of Competing Interest

The authors declare that they have no known competing financial interests or personal relationships that could have appeared to influence the work reported in this paper.

Disclosures

None

Keywords

Microfluidics; Microfluidic artificial lung; Biomaterials; Biocompatibility; Thrombosis

1. Introduction

Artificial lungs (ALs) have been used in the clinic for several decades to supplement lung function when the native lung is compromised due to disease or injury [1,2]. To date, ALs have been primarily employed in clinical scenarios including: 1) during cardiopulmonary bypass in cardiac surgery or 2) during extracorporeal membrane oxygenation either as a bridge-to-transplant (to replace the natural lung) or as a bridge-to-recovery (to allow the natural lung to heal). The use of ALs is increasing as research continues to show clear benefits compared to traditional treatments and as more hospitals are equipped to provide such care [3].

Current clinical ALs are based on hollow-fiber technology, in which blood flows through a bundle of hollow fibers while a sweep gas is delivered through the inside of the fiber lumens, facilitating gas diffusion through the walls of each fiber (Fig. 1). Despite the clinical success of hollow-fiber ALs, there are several draw-backs inherent to the design that limit the achievable gas exchange rates and overall effectiveness [4]. These inherent inefficiencies result in gas exchange that is sub-optimal compared to the natural lung.

The use of hollow-fiber oxygenators is currently limited to ICU use for patients at rest [5,6]. Biocompatibility remains one of the major challenges in managing patients being treated with ALs. Blood contact with the foreign surfaces within AL circuits causes platelet activation, inflammation, and initiation of the coagulation cascade [4]. To mitigate this foreign body response, patients are given systemic anticoagulation, which often results in poor outcomes due to bleeding complications [3]. Despite continued progress in the engineering of hollow-fiber based ALs and their expanded use in the hospital setting, there is an urgent need to develop better AL technologies, both to improve currently used treatments and also to reach patient populations for which treatment with ALs is currently not available.

Microfluidic artificial lungs (μALs) can potentially replace hollow-fiber technologies because of the ability to create μALs with comparably higher gas exchange efficiency and precisely defined blood flow paths [4]. By creating artificial capillaries and gas exchange membranes with sizes on the order of microns or tens of microns, μALs can achieve gas exchange efficiencies approaching or even exceeding that in the natural lung [4,7–9]. This can result in μALs that, like the natural lung, only require atmospheric air to fully oxygenate blood moving through the device, which would improve safety and portability by removing the need for a compressed O_2 tank and possible complications associated with high O_2 concentrations in the blood [10]. Priming volumes in μALs can be significantly reduced compared to traditional ALs, which is desired as reduction of priming volume has been associated with improved outcomes in cardiopulmonary bypass procedures [11–13]. The blood flow paths in μALs are generally much less tortuous than in hollow-fiber oxygenators, which can help to reduce thrombus formation. Additionally, blood flow networks in μALs

can be designed using physiological branching principles [10,14], and can thus present physiological shears/pressures to blood cells, potentially improving blood compatibility.

However, micron-scale artificial capillaries may be more susceptible to blockage due to clotting than traditional devices with larger diameter blood flow paths. Additionally, although the large surface area to volume ratios (SA/V) in μALs results in efficient gas exchange, it also ensures that essentially all the blood cells moving through the device will be in direct contact with a foreign surface. The resulting foreign body response can result in unwanted thrombus formation, thromboemboli, platelet consumption and activation, leukocyte activation, and inflammation. *Thus, a major hurdle for the development of μALs is the ability to create biocompatible devices, both for device lifetime concerns and also to minimize deleterious systemic effects to the patient*.

A common strategy to improve biocompatibility involves coating the blood-contacting surface with something that renders the surface bioinert or biocompatible. Numerous surface coating strategies have been investigated in pursuit of a truly non-thrombogenic biomaterial. These strategies include highly hydrophilic or hydrophobic surfaces, zwitterionic polymers, protein-coated surfaces (such as albumin), cultured endothelial cell coatings, immobilized anticoagulants (such as heparin or argatroban), and others [15,16]. Polyethylene glycol (PEG) is one such coating that has been studied extensively and is used in this study. PEG is a hydrophilic molecule that results in general surface passivation to prevent the adsorption of plasma proteins and platelets on the blood-contacting surface.

Researchers are also exploring strategies for biocompatibility that involve the use of nitric oxide (NO) [17–24]. NO is an important modulator of vascular homeostasis and among its many biological functions is the inhibition of platelet adhesion/aggregation. The elution of NO from blood-contacting surfaces has been shown to be beneficial in situations in which blood activation and thrombus formation are a concern, particularly with indwelling catheters or sensors [25–30]. NO can be supplied to a blood-material interface in a PDMS device by incorporating an NO-eluting molecule into the base polymer comprising the device, or by coating the surface with an NO-eluting coating. Unique to ALs, the sweep gas also provides a convenient vehicle with which to deliver NO directly to the blood moving through the device.

NO treatment can potentially be more effective in μALs than in traditional hollow fiber devices for some of the same reasons that gas exchange (O_2 and CO_2) is more efficient in μALs. First, the large gas exchange surface area to blood volume (SA/V) ratio results in very efficient NO diffusion into the blood. Also, the small diameter channels allow NO to be delivered locally to the platelets and leukocytes, which is important due to the short half-life of free NO in blood. Free NO in blood is rapidly converted to nitrite and nitrate via oxidation by oxyhemoglobin, so competition of leukocytes and platelets with red blood cells which would scavenge available NO may reduce effectiveness of the treatment. Conveniently, leukocytes and platelets are pushed to the edge of flow in whole blood, keeping these cells in close contact with the membrane through which the NO is delivered. In very small microchannels this forced margination is diminished as cells more or less

travel in single file, however in this case the diffusion distance for NO to travel to interact with platelets/leukocytes is still small.

As the field of μALs is still relatively new, studies of biocompatibility within functioning μALs are limited. We have previously reported that μALs with a hydrophilic PEG coating displayed a significant reduction in coagulation response and significantly improved gas exchange compared to uncoated μALs when challenged *in vitro* with citrated human platelet-rich plasma (PRP), citrated bovine whole blood, or heparinized porcine whole blood [14,31]. Gimbel et al. demonstrated an improvement in blood compatibility of μALs which are seeded with a confluent monolayer of endothelium compared to uncoated devices when challenged *in vitro* with heparinized bovine blood [32]. While *in vitro* tests are useful, *in vivo* testing will be required as we move toward developing truly biocompatible μALs. In addition to providing a more rigorous and physiologically-relevant challenge, live animal models are required to determine the response of the animal to the extracorporeal device. Very few biocompatibility studies have been done using functional μALs in an *in vivo* setting. We previously demonstrated the use of a PEG-coated μAL for 3h using a rat model [14], and Rochow et al demonstrated the use of a microfluidic oxygenator array in a newborn piglet model [33]. Both studies were demonstrations in single animals and did not achieve statistical significance. In developing μALs for clinical application, it will be necessary to further study how biocompatibility affects thrombosis in the device, device lifetime, and systemic effects to the patient caused by blood contact in the device.

The purpose of this study is to evaluate the biocompatibility of small-scale μALs and to explore the potential of two strategies for improving biocompatibility, both in an *in vitro* benchtop experiment and an *in vivo* rabbit model. The strategies investigated in this work include a hydrophilic surface coating (PEG) to reduce/inhibit platelet and plasma protein deposition, the addition of NO to the sweep gas in order to inhibit platelet and leukocyte activation within μALs, and the combination of these two approaches. This study is the first study to: 1) investigate the effect of NO release on biocompatibility in a microfluidic network; 2) combine a hydrophilic PEG coating with NO release to improve blood compatibility; 3) perform extended *in vivo* biocompatibility testing of a μAL.

2. Methods

2.1. μAL Design

Two μAL designs were used in this study. *In vitro* testing was performed using a small-scale device intended to support up to 2 mL/min of blood flow. The resulting devices had three channel heights: 1) a branching distribution network of 180 and 60 μm heights and 2) artificial capillaries of 12 μm height. The membrane thickness used in this study was 50 μm, and the priming volume of this device was 92 μL.

In vivo hemocompatibility testing was performed using a previously-published design which has a branching distribution network with 250 μm channel heights, 30 μm tall capillaries, a blood priming volume of 400 μL, and an achieved rated blood flow of 17 mL/min [8]. This device was chosen for *in vivo* testing as its low resistance enabled operation in an arteriovenous (AV) configuration, eliminating any possible complications due to a blood

pump. The rated flow of the device allowed the total blood flow of the animal to be perfused approximately every 10-20 minutes, enabling the quantification of systemic effects through measured blood parameters. The full description of this design is available in the cited work [8]. Top view computer-aided design (CAD) drawings of both designs are shown in Fig. 2.

2.2. Device Fabrication and Coating

The μALs used in the study are composed of polydimethyl siloxane (PDMS, Sylgard® 184 silicone elastomer) and were made using standard photolithographic molding methods. Briefly, molds consisting of the negatives of the device features were built on silicon wafers (University Wafer, Boston, MA) using negative photoresist (MicroChem SU-8). Photoresist was spun to desired thickness using a Specialty Coating Systems spin coater, baked for appropriate times based on layer thickness (see MicroChem SU-8 datasheet), exposed to UV light using a Kinsten KVB-30D UV exposure unit while covered with photolithography mask (FineLine, Colorado Springs, CO), and developed using SU-8 developer (MicroChem). Sylgard® 184 silicone elastomer base and curing agent (10:1, Dow Corning) were mixed, degassed, poured over the previously-created silicon molds for the blood and gas flow networks, and baked at 80°C for 45 min. The membrane was formed by spinning PDMS to the desired thickness on an acrylic disk using the spin coater. The cured device parts (blood network, gas network, membrane) were assembled using O_2 plasma bonding by first bonding the blood network to the membrane, and then bonding the gas network to the other side of the membrane. Inlet/outlet ports made from segments of 1/8” inner diameter (ID) silicone tubing were added to allow access to the blood and gas networks to form the finished device.

To form devices which are coated with PEG, the inlet/outlet ports are added to the blood/gas networks prior to bonding to the membrane. Immediately upon bonding the blood network to the membrane (i.e. while the surface is still activated by the O_2 plasma), PEG solution was added to the blood flow network and allowed to react for 1 hr before rinsing with deionized water and drying. A more complete description of both the fabrication of PDMS μALs and the PEG coating method can be found in the cited works [8,34].

2.3. X-ray photoelectron spectroscopy (XPS)

X-ray photoelectron spectroscopy was used to characterize the PEG-coated surfaces using the standard uniform overlay model [35]. Briefly, simple rectangular PDMS chambers were prepared using a thin acrylic rectangle as the mold for the flow chamber with 1/8” ID silicone tubing segments used as inlet/outlet ports. PEG coating was performed as described in the previous section. Samples of uncoated PDMS and PEG-coated PDMS surfaces were sent for XPS analysis at the Michigan Center for Materials Characterization (Ann Arbor, MI) using a Kratos Axis Ultra XPS (Kratos Analytical, Manchester, UK) with a monochromatic Al Kα source and an X-ray incidence angle of 54.7°. Survey scans as well as high resolution scans of the C-1s peak were performed in order to confirm presence of the PEG coating and determine the conformation of the PEG coating. PEG coating conformation was determined by calculating the average distance between PEG chains and the Flory radius. The ratio between these two values determines whether PEG chains are

fully extended in the desired brush conformation, with $R_f/L > 1.0$ indicating the PEG coating is in the brush regime [36,37].

The distance between PEG chains, L (nm), was calculated using Eqs. 1–3 [38],

$$I = I_0\left(\frac{t}{E_L \sin\theta} - 1\right) \quad (1)$$

Where I and I_0, respectively, are the intensities (eV) of the C-1s peak on the PEG-coated and uncoated samples, t is the thickness (nm) of the PEG coating, and θ is the X-ray incident angle (deg). E_L is the electron attenuation length (nm) of the C-1s peak, calculated by Eq. 2 [39],

$$E_L = \frac{49}{E^2\rho} + 0.11\frac{\sqrt{E}}{\rho} \quad (2)$$

where E is energy (eV) of detected electrons from the C-1s peak (calculated as the difference between the X-ray core energy and the core-binding energy of C), and ρ is the density of PEG (1.1 g/cm^3). The thickness of the PEG layer, calculated from Eqs. 1 and 2, is used to calculate the approximate distance between PEG chains using Eq. 3 [38],

$$L = \sqrt{\frac{M}{t\rho N_A}} \quad (3)$$

where M is the molecular weight (g/mol), and N_A is Avogadro's number (6.023×10^{23} / mol). The Flory radius, R_f (nm), is calculated by Eq. 4 [40–42],

$$R_f = aN^{0.64} \quad (4)$$

where a is the size of a monomer unit and N is the degree of polymerization of PEG.

2.4. Platelet-rich plasma (PRP) preparation

Citrated bovine platelet-rich plasma (PRP, Lampire, Pipersville, PA) was warmed to 37°C in a water bath. Aqueous calcium chloride (400 μL of 5% w/v) was added to a 10 mL sample of the PRP in order to fully counteract the citrate anticoagulant. This sample was then used to determine the heparin dose (per volume of blood) required to achieve an active clotting time (ACT) between 300-400 s (measured via an Abbott Point of Care iSTAT Handheld Blood Analyzer).

The required heparin dose (between 2.5-5 USP units/mL PRP depending on the specific PRP batch) was then added to the stock of citrated bovine PRP that will be used in the *in vitro* hemocompatibility flow testing, such that when the citrate anticoagulant is counteracted by calcium chloride, the resulting PRP will have the desired ACT. The tubing circuit described below is designed such that citrate is added to the PRP directly upstream of the device inlet, minimizing the exposure of inlet tubing to clottable PRP prior to entering the device.

2.5. In Vitro NO Flux Measurement

The same μAL design and bench setup used in the *in vitro* hemocompatibility testing was used to test NO flux across the membrane. Saline was flowed through devices at 0.4 mL/min and 2000 ppm NO sweep gas was supplied at 2 mL/min. Samples of saline from the outlet of the μAL were collected. The NO content of saline samples was estimated using the ozone-chemiluminescence method (GE Sievers 280i Nitric Oxide Analyzer, NOA) [43]. After collection, samples were stored frozen in air-tight glass vials until analyzing. As the primary oxidation product of NO in the presence of oxygen is nitrite, the total NO content was measured after reduction of nitrite back into NO in acidified KI solution. The nitric oxide analyzer was calibrated with 0 ppm NO calibration gas and 43.2 ppm NO calibration gas. 2 mL of 0.2 M H_2 SO_4 and then 2 mL of 0.2 g/mL KI were added into a glass NOA cell equipped with a septum, and after stabilization of the baseline, 20 μL of sample solution was injected using a gas tight Hamilton syringe. NO was purged out from the solution phase by bubbling nitrogen through the solution. To get the total NO content of the sample, the registered NO signal was integrated between two injections and the area under the curve was multiplied by an NOA constant, which was determined with a standard solution with known nitrite concentration. Each sample was measured in at least triplicate.

2.6. In Vitro Hemocompatibility Testing

The prepared PRP was loaded into a 60 mL syringe, then delivered to a small-scale μAL via a syringe pump and 1/8” ID silicone tubing. A three-way stopcock was placed immediately upstream of the μAL inlet. This stopcock was used to continually infuse the flowing PRP with aqueous calcium chloride in order to fully counteract the citrate anticoagulant, resulting in PRP entering the device which is pre-heparinized to the desired ACT. A syringe pump was used to deliver 0.2 mL/min of PRP to the μAL, and a second syringe pump was used to deliver 20 μL/min of aqueous calcium chloride (5% w/v) to the PRP stream at the inlet of the μAL. Blood pressure was monitored using flow-through pressure sensors (Honeywell 26PC Series) at the inlet and outlet of the μAL. PRP was flowed through the μAL for 2 hrs and flow resistance (pressure drop/blood flow rate) was used as an indicator of clot formation within the device. Sweep gas at a rate of 2 mL/min was delivered to the gas network of the μAL from compressed gas tanks using silicone tubing and a mass flow controller (Omega, model FMA5502). Sweep gas used in these studies was either pure nitrogen, or NO-supplemented nitrogen (500 or 2000 ppm NO in balance N_2). For ease of experimental control, an inert carrier (N_2) was used as the sweep gas so that the amount of NO delivered to the device is controlled, as NO can react in the presence of O_2 - potentially reducing the concentration of NO in the sweep gas. Fig. 3 shows a schematic of the experimental setup used for *in vitro* hemocompatibility testing.

2.7. In Vivo Hemocompatibility Testing in Rabbits

For this study we chose to use a rabbit model because it has hemostatic similarities to humans providing a relevant thrombotic challenge to the device. Additionally, the blood volume in the rabbit is large enough to allow for several blood draws throughout the experiment, while being small enough to detect systemic effects to the animal due to the μAL. Compared to smaller animals, the vessel size of rabbits make them easier to cannulate

and less likely to clot in the cannula site. Compared to larger animals, the rabbit model is more cost effective and size-appropriate for the current blood flow capacity of μALs.

Blood compatibility in μALs was tested in adult, white New Zealand rabbits (2.5-3.5 kg) and a previously-published μAL design which has a rated blood flow of 17 mL/min [8]. The device was connected to the animal via an arteriovenous (AV) circuit between the carotid artery and jugular vein. This configuration was used because it does not require the use of a blood pump; the natural pressure drop between the blood drainage from the animal (carotid artery) and reinfusion to the animal (jugular vein) drives flow through the device. This is advantageous as it removes any effects on the blood or the animal due to the presence of the blood pump that would otherwise confound effects caused by the μAL.

All procedures were performed in accordance with institutional IACUC-approved protocols. Rabbits were anesthetized using inhaled isoflurane via nose cone prior to performing a tracheotomy to enable endotracheal ventilation. Animal body temperature was monitored throughout the experiment with a rectal probe and temperature was maintained using a heat lamp and/or a water-jacketed heating blanked when needed. An IV catheter placed in either the left or right marginal ear vein was placed and used to administer Lactated Ringer's (LR) solution to maintain blood pressure stability and also to administer a continuous infusion of heparin to achieve an ACT of 350±50 sec. A surgical dissection was performed to expose the left and right carotid artery. The right carotid artery was cannulated to monitor blood pressure and for blood sample collection. The drainage cannula for the extracorporeal circuit was placed in the left carotid artery and the reinfusion cannula is placed in the left external jugular vein. A saline-primed extracorporeal circuit consisting of 1/16" ID silastic laboratory tubing, a μAL, and a 3-way stopcock is connected to the drainage and reinfusion cannulas. Flow through the circuit was opened and blood flow was driven through the μAL by the pressure difference between arterial and venous pressure. Sweep gas consisting of either 1000 ppm NO (balance N_2) or pure N_2 at a rate of 20 mL/min was delivered to the gas network of the μAL from compressed gas tanks using silicone tubing and a mass flow controller (Omega model FMA5508). For ease of experimental control, an inert carrier (N2) was used as the sweep gas so that the amount of NO delivered to the device is controlled, as NO can react in the presence of O_2 - potentially reducing the concentration of NO in the sweep gas. Blood is drawn every 60 min to evaluate platelet/leukocyte count (in some cases blood samples were drawn every 30 min for devices which appeared to be failing early in the experiment due to clotting). Blood samples were analyzed using a ProCyte Dx Hematology Analyzer (Idexx Laboratories Inc., Westbrook, Maine) to obtain platelet and leukocyte counts. As normal platelet/leukocyte counts may vary between animals, platelet/leukocyte data are reported as percentage of baseline. Baseline blood data was obtained once the cannulations have been completed and the ACT is confirmed to be within the desired range, but prior to opening blood flow through the device and extracorporeal tubing. Device blood flow was monitored using a flow probe (Transonic Model 1PXN inline flow sensor) or by timed blood draining into a tared vial for 10 s and weighing. Experiments were run for 4 hr or were terminated early if device blood flow had reached the low limits of our detection methods (for the flow probe this was measured blood flow ≤ 0.1 mL/min, for the drip method this was when less than 2 drops of blood were produced per 10 s). After the experiment, devices were immediately flushed with 2 mL/min saline for 5 min.

2.8. Image Analysis

Devices were imaged in order to estimate the % area containing residual blood components after flushing. Images of flushed μALs following *in vivo* testing were processed using ImageJ software. Images were cropped the approximate area containing the blood flow network. Color thresholding was used to select all red hues within the blood flow network area. The “Analyze particles” function was used to quantify the percentage of the cropped frame above the color threshold for red hues.

2.9. Data and Statistical Analysis

For *in vitro* testing, device resistance was measured every 10 minutes for 2 hours. Device resistance vs. time is presented in Fig. 4 (top) as the average resistance (± standard error) at each timepoint. Linear regression was used to calculate the slope of device resistance vs. time for each device. The slopes of device resistance vs. time for each group were averaged and compared using one-way analysis of variance (one-way ANOVA) using Dunnett’s post hoc test for multiple comparisons, using GraphPad Prism 8.4.1 (San Diego, CA). Differences were deemed significant for $p<0.05$. All reported experiments were performed in at least triplicate.

For *in vivo* flow resistance tests, the flow resistance vs. time curves were primarily non-linear, as device failure occurs rapidly once clotting begins to occur in the devices in this setting. Thus, rather than comparing flow resistance or the linear slope of increasing flow resistance, the time to failure for each group was averaged and compared. A two-way ANOVA with post hoc Fisher’s LSD test was used to determine whether differences between groups were significant. Four hours was used as the time to failure for devices which lasted the duration of the 4 hr experiment, regardless of whether the device actually failed at that time, so that a statistical comparison could be performed between the groups. Differences were deemed significant for $p<0.05$. All reported experiments were performed in at least triplicate.

The estimated percent clot area in the flushed post-experiment devices for each group were averaged and compared to other groups using a two-way ANOVA with post hoc Fisher’s LSD test.

Statistical analysis of the effect of coatings and/or nitric oxide on cell count was performed for all data gathered prior to or at the 1-hour timepoint (due to availability of data, as many devices had failed by 1 hour). If a dataset had an entry for both the 30 minute and 1 hour timepoint, only the 1 hour timepoint was used for the statistical analysis. As the baseline platelet and leukocyte concentration varies between animals, the percent change in cell count relative to baseline was plotted and the means of these values were used in statistical testing. Statistical analysis of platelet/leukocyte count data was performed using a two-way ANOVA with post hoc Fisher’s Least Significant Difference test. Differences were deemed significant for $p<0.05$.

3. Results

PRP flow through the μAL resulted in a steadily increasing resistance to flow over 2 hr. However, the addition of NO to inert sweep gas (500 or 2000 ppm) significantly slowed this increase in resistance (Fig. 4). There was no apparent difference between the use of either 500 or 2000 ppm. The achieved flux of NO through the 50 μm thick membranes used for biocompatibility testing was $7\pm2 \times 10^{-10}$ mol NO•min^{-1}•cm^{-2} for 2000 ppm NO sweep gas (Fig. 4). The NO flux across a thinner membrane (20 μm) was not significantly different than that across the 50 μm membranes.

XPS data along with contact angle measurements confirmed the successful coating of the PDMS surface with PEG (Fig. 5). The high resolution C-1s scan of the PEG-coated surface shows a clear increase in the peak corresponding to C-O bonds compared to the uncoated PDMS surface, indicative of successful PEG grafted to the surface [35,38,39]. The distance between PEG chains was estimated to be 0.32 nm and the Flory radius for the PEG is 1.27 nm. The ratio of the Flory radius to the average distance between PEG chains (≅4) indicates that the PEG coating is in the brush conformation.

In an AV rabbit ECMO circuit, neither NO sweep gas nor PEG coating alone significantly extended the device lifetime compared to controls (Fig. 6). However, the combination of PEG surface coating with NO sweep gas significantly improved device lifetime (Fig. 6) – with 4 of 6 trials lasting the entire 4 hr experimental time. The time to clot for the PEG+NO group is a conservative estimate used for statistical comparison to controls, as the experiments were stopped at 4 hr although devices were still functioning at that time.

There was significantly less surface coverage of gross clot within the PEG+NO devices compared to uncoated devices after flushing the μALs with saline to remove non-adherent blood components (Fig. 7). There was no statistical difference of platelet or WBC counts in the live animal during the 4 hr test (as % relative to baseline) between groups (Fig. 8). However, devices which received N_2 sweep gas displayed an apparent decrease in systemic platelet count upon exposure to blood compared to devices which received NO sweep gas. Relative WBC count remained near baseline for all groups upon exposure to blood, except for the UC+N_2 group which displayed an apparent decrease in systemic WBC count within the first hour prior to device failure.

4. Discussion

Multiple hurdles must be overcome before μALs are ready to be tested in human trials and eventually available for widespread clinical use. The first is the lack of a reliable method by which to fabricate large scale devices capable of supporting human scale blood flows. A simple, scalable, and cost-effective method of repeatably producing μALs which can handle liters per minute of blood flow will be required to achieve the widespread use of μALs for all the potential clinical applications. There has been considerable effort by the research community in recent years to overcome this limitation [8,33,44–52].

Biocompatibility is an equally important barrier which must be overcome in order for μALs to be used clinically. First, device lifetime will be limited if they are prone to clot formation

within the blood flow network. While thrombogenic devices may still be usable in acute settings in which the patient is anticoagulated, the eventual goal is to be able to use these devices for extended periods with little or no anticoagulant. Any blood activation can be problematic for the patient as well. In this regard, μALs may potentially be advantageous as further development and scaling up is expected to result in smaller priming volumes and surface areas than hollow-fiber oxygenators [4,9]. However, μALs will have a higher SA/V ratio, ensuring that essentially all the blood moving through the device contacts a foreign surface.

Strategies for improving biocompatibility of μALs have included careful design of the blood flow network and modification of the blood-contacting surfaces to mitigate the foreign body response. Blood flow networks for μALs have been designed to mimic the natural branching angles and relative vessel sizes found in physiological vasculature and other naturally-occurring branching systems in order to ensure controlled levels of wall shear stress, flow velocities, and pressures experienced by blood within these devices [8,14,46,49,50]. The prevailing hypothesis in the field is that biocompatibility can be improved by controlling these hemodynamic parameters, though most studies involving functional μALs to date have focused on gas exchange performance rather than biocompatibility. Early studies regarding biocompatibility of μALs and the effect of blood flow network design on thrombosis displayed mixed results. In a study by Vollmer *et al.*, thrombus deposition and channel occlusion occurred in small-scale μALs when challenged with anticoagulated blood particularly near branching points [53], however in a study by Gilbert *et al.* which utilized computer simulation to ensure uniform flow properties in the μALs, thrombosis was not visible following 6-12 hrs of anticoagulated bovine blood flow [54]. This discrepancy illustrates the hypothesis that biocompatibility of μALs can be improved through careful design of the blood flow network, though these studies were done with anticoagulated blood and in a benchtop setting rather than in live animals. In more physiological, thrombogenic systems, further modifications such as surface coatings or locally-introduced antithrombotic agents will be required to produce a truly biocompatible μAL capable of perfusing blood with little or no anticoagulant for an extended period of time (weeks to months), particularly due to the inherently high SA/V ratios in microfluidic devices.

There have been a multitude of studies focused on improving hemocompatibility of surfaces composed of PDMS [55], the most common material used to make μALs. However, few studies have been done to apply these strategies and assess their effectiveness in networks of microchannels, and even fewer in functioning μALs. In 2002, Borenstein *et al.* introduced the possibility of improving hemocompatibility by seeding endothelial cells into microchannels [56]. In 2009, Burgess *et al.* applied this strategy and demonstrated the ability to culture endothelial cells in μALs, however no hemocompatibility studies were presented [57].

In 2013, Zhang et al coated rectangular microchannels with zwitterionic polybetaine which renders the surface highly hydrophilic [58]. When challenged with heparinized bovine blood, uncoated devices occluded due to thrombi within 1 hour while coated devices displayed significantly decreased thrombus formation over the same time period. In 2014, Kovach *et al.* used a PEG coating to improve hemocompatibility of μALs and tested these

devices using heparinized porcine blood for up to 19 hours, and found that blood flow resistance in PEG-coated devices took over 16 times longer to double than in uncoated devices and contained significantly less deposited clots following the blood challenge [31].

Researchers are also exploring strategies for biocompatibility that involve the use of nitric oxide. NO is an important modulator of vascular homeostasis and among its many biological functions is the inhibition of platelet adhesion/aggregation [17–24]. The elution of NO from blood-contacting surfaces has been shown to be beneficial in situations in which blood activation and thrombus formation are a concern, particularly with indwelling catheters or sensors [25–30]. NO has also been shown to be effective in reducing thrombogenicity in hollow-fiber artificial lungs [59,60]. It stands to reason that NO may also be effective in μALs, or even more effective due to the high surface area to blood volume ratio, though to date this has not been tested. Recently, the Cook group presented a multimodal approach to improve hemocompatibility which combined surface coatings to reduce surface fouling with NO release to promote platelet quiescence [61,62]. Gupta *et al.* used a poly-2-methoxyethylacrylate coating combined with NO release (100-1000 ppm) which resulted in significantly less platelet deposition on gas-permeable polypropylene membranes compared to controls when challenged with ovine PRP [62]. Amoako *et al.* used a zwitterionic polycarboxybetaine surface coating combined with NO release to study the effect on platelet adhesion to a PDMS membrane when challenged with ovine PRP [61]. Compared to uncoated controls with no NO release, uncoated devices receiving NO (100 ppm) displayed reduced platelet adhesion (80% of the platelet adsorption seen on controls) while membranes that had both a coating and NO release displayed an even more dramatic decrease (less than 7% of the control level of platelet adhesion). This approach of using a surface coating combined with NO release has yielded promising results, but prior to this study had yet to be applied to the context of μALs.

More biocompatibility studies within functioning μALs and with live animals are required to understand just how the unique μAL geometries affect blood/material interactions and the effectiveness of various strategies to improve biocompatibility. Here, we present *in vivo* biocompatibility testing of small-scale μALs which have a surface coating of PEG, supplemental NO introduced to blood via the sweep gas, or both. Prior to *in vivo* testing, a pilot study consisting of an *in vitro* bench test was performed to assess the effectiveness of NO treatment at varied sweep gas concentrations. This study is the first to: 1) investigate the effect of NO release on biocompatibility in a complex microfluidic network; 2) combine a hydrophilic PEG coating with NO release to improve blood compatibility; and 3) perform extended *in vivo* biocompatibility testing of a μAL.

In this study, we investigate the effectiveness of NO-doped sweep gas in improving device lifetime when challenged with clot-table blood both *in vitro* and *in vivo*. Prior to biocompatibility testing, we performed preliminary experiments to estimate the flux of NO across the membrane and into blood within the μAL. The flux of NO across the membrane can be controlled by setting the concentration of NO in the sweep gas. Additionally, NO flux in μALs will depend on membrane thickness and composition, as well as any potential effect due to the presence of a surface coating. It is important to understand exactly how much NO needs to be delivered to produce the desired result, in particular because the SA/V in μALs

allows for very efficient local delivery of NO. Too little NO delivered to the blood may not improve biocompatibility at all while too much NO may cause blood methemoglobin levels to rise (methemoglobinemia), which can impair the ability of hemoglobin to carry O_2 and CO_2 [63,64]. Healthy endothelium has been estimated to produce NO at rates between 0.5-4 $\times 10^{-10}$ mol cm^{-2} min^{-1} [65,66], so this is likely a good starting point to determine the required dose of NO to be effective in improving μAL biocompatibility. The concentrations of NO in the sweep gas used in this study were chosen to be near this physiological range of NO flux.

In this study, we see that the addition of NO (500 or 2000 ppm in N_2 sweep gas) in uncoated μALs does prolong device lifetime compared to control devices when challenged with heparinized bovine PRP. The rate of increasing resistance in the devices was the same whether 500 or 2000 ppm NO was used. The flux of NO across the μAL membrane provided by 2000 ppm NO sweep gas in these devices was about 7×10^{-10} mol cm^{-2} min^{-1} , slightly larger than estimated physiological values.

When μALs were challenged in an *in vivo* rabbit model, the addition of NO alone (1000 ppm in N_2) did not result in a significant improvement in device lifetime compared to controls. There are several reasons which may account for this result. The current μAL design is such that NO is only introduced from one of the blood-contacting surfaces in the blood channels. Samples of devices were analyzed under microscope to see if the NO-eluting surface was less fouled than the other surfaces, however no discernable trend was noticed in this study. This can possibly be attributed to the fact that most devices were operated until failure, that is until thrombus had already occluded the channels. It is possible that inspections at earlier time points may have found less platelet deposition on NO-eluting surfaces, although this is entirely speculative at this point. Finally, the live rabbit model is qualitatively more thrombogenic than the *in vitro* testing done in this and other studies. With larger sample size, a significant improvement in device lifetime may become apparent in NO-eluting devices, though for practical purposes a small improvement compared to controls in this setting may not translate to a meaningful difference in biocompatibility clinically in humans.

In this study, a PEG coating alone did not significantly improve device lifetime compared to uncoated controls when a live rabbit is used to challenge the devices. We expected to see a significant increase in device lifetime based on previous *in vitro* data by our lab and other labs which demonstrate reduction in protein/platelet deposition with a PEG coating [14,34,67]. XPS analysis confirmed that the PEG coating was successfully applied to the surface and that the PEG chains are in the brush conformation, yet a significant improvement in device lifetime compared to uncoated controls was not observed. There are several potential explanations as to why this was the case. One potential cause of this discrepancy may simply be due to the high thrombogenicity in the live rabbit model serving as a more substantial challenge to the coating strategy than less physiological *in vitro* studies. Another potential factor is the quality of the PEG coating. The XPS data provides a representative sample of the coated surface, however it cannot ensure that all of the blood-contacting surfaces were evenly coated. Any gaps due to air bubbles or incomplete filling during the liquid-phase PEG-coating reaction can result in blood-contacting surfaces

that are uncoated, which could then be a location where clot can initiate. Care was taken to fully fill the blood channels and avoid air bubbles during the coating procedure, however given the results we speculate whether gaps in the PEG coating may have contributed to less thromboresistance than expected. It should also be pointed out that on average, the PEG group had a longer device lifetime than controls, but differences were not significant. With an increased sample size, significance between the PEG and control groups may be achieved. Our power analysis prior to experimentation predicted that this sample size would produce significance between experimental and control groups, however differences between this experiment and previous data may have underestimated the required sample size.

When both a PEG surface coating and NO sweep gas were used together in *in vivo* tests, the device lifetime significantly improved, despite the fact that each strategy individually displayed little effect on our primary endpoint (time until device failure). The majority of devices in the PEG+NO group (4 of 6 trials) lasted the entire 4 hr test period, while the devices in the control group ($UC+N_2$) generally failed within 30 minutes upon exposure to blood. In this study we see the most benefit in the PEG coated devices with NO, presumably because PEG and NO are addressing two of the most relevant clotting contributors (surface fouling and platelet/leukocyte activation). However, the devices which are PEG-coated should have a lower amount of surface fouling by plasma proteins compared to uncoated devices, which can reduce/minimize platelet activation due to surface adsorption or release of platelet agonists. It appears that clotting in the groups which did not contain NO release was accompanied by a decrease in platelet count (Fig. 8) presumably due to platelet consumption within the device, though differences in platelet counts were not statistically significant. Platelet consumption in devices which were uncoated but received NO appeared to be minimal, as the baseline platelet concentration was maintained throughout the experiment. However, these devices failed due to clotting also (possibly due to fibrin clots), illustrating the need for both the surface coating and NO. It is unclear in this study exactly how much the presence of PEG improves the effectiveness of the NO treatment, as the effect on our primary endpoint is not noticeable unless both PEG and NO are present. However, these results agree with multiple studies from the Cook Group (Carnegie Mellon University) which show that the combination or anti-absorptive coatings with NO release is dramatically more effective in reducing platelet adhesion than either strategy alone [61,62].

Moving forward, it will be important to optimize each strategy to maximize the efficacy of the combined strategy. This will include careful optimization of the PEG coating such that an optimal conformation is achieved uniformly across the surface, and determination of the optimal NO flux across the membrane and, ideally, from all blood-contacting surfaces in the device. In future studies we will identify the range of NO delivery in μALs that results in marked improvement in biocompatibility while causing no deleterious systemic effects. Additionally, we are investigating other types of surface coating strategies which may work well in conjunction with supplemental NO treatment.

5. Conclusions

Nitric oxide doped sweep gas in combination with a hydrophilic PEG coating extends the lifetime of μALs in rabbits. A PEG coating or NO sweep gas alone did not significantly

increase device lifetime when challenged with clottable blood using an *in vivo* rabbit model. Reducing protein deposition and platelet activation (ideally locally in the device so as not to affect systemic platelet function) are likely both necessary to produce μALs which are highly hemocompatible over extended periods of time.

Acknowledgments

Thanks to the ECLS Lab for generously providing lab space, supplies, and expertise in the development and carrying out of the *in vivo* testing. Thanks to Elyse Fleck for the help she provided with the planning and preparing of the manuscript.

The authors acknowledge the University of Michigan College of Engineering and NSF grant #DMR-0420785 for financial support and the Michigan Center for Materials Characterization for use of the Kratos Axis Ultra XPS and technical support. The authors would like to thank Nancy S. Muyanja for assistance in performing the described XPS analysis.

Funding

This work was supported by Department of Veterans Affairs Rehabilitation Research and Development (VA RR&D) Award # I01RX000390. The contents do not represent the views of the U.S. Department of Veterans Affairs or the United States Government.

References

[1]. ECLS Registry Report: International Summary, Extracoreporeal Life Support Organ. (2019). https://www.elso.org/Registry/Statistics/InternationalSummary.aspx (accessed August 5, 2019).

[2]. Yeager T, Roy S, Evolution of Gas Permeable Membranes for Extracorporeal Membrane Oxygenation, Artif. Organs (2017) 10.1111/aor.12835.

[3]. Makdisi G, Wang IW, Extra Corporeal Membrane Oxygenation (ECMO) review of a lifesaving technology, J. Thorac. Dis (2015) 10.3978/j.issn.2072-1439.2015.07.17.

[4]. Potkay JA, The promise of microfluidic artificial lungs, Lab Chip 14 (2014) 4122–4138 10.1039/C4LC00828F. [PubMed: 25198427]

[5]. Federspiel WJ, Henchir KA, Lung, artificial: basic principles and current applications, Encycl. Biomater. Biomed. Eng. LZ (2004) 10.1081/E-EBBE.

[6]. Nolan H, Wang D, Zwischenberger JB, Artificial lung basics: Fundamental challenges, alternative designs and future innovations, Organogenesis (2011) 10.4161/org.7.1.14025.

[7]. Potkay JA, A high efficiency micromachined artificial lung, in: TRANSDUCERS 2009 - 15th Int. Conf. Solid-State Sensors, Actuators Microsystems (2009) 2234–2237 10.1109/SENSOR.2009.5285592.

[8]. Thompson AJ, Ma LJ, Plegue TJ, Potkay JA, Design Analysis and Optimization of a Single-Layer PDMS Microfluidic Artificial Lung, IEEE Trans. Biomed. Eng (2019) 10.1109/TBME.2018.2866782.

[9]. Potkay JA, Wagner G, Kaesler A, Steinseifer U, Schmitz-Rode T, Arens J (Eds.), Reply to the "Comment on 'the promise of microfluidic artificial lungs'", Lab Chip 16 (2016) 1274–1277 Lab Chip. 16 (2016) 10.1039/c6lc00221h, doi:10.1039/C5LC01508A. [PubMed: 26957040]

[10]. Potkay JA, Magnetta M, Vinson A, Cmolik B, Bio-inspired, efficient, artificial lung employing air as the ventilating gas, Lab Chip 11 (2011) 2901–2909 10.1039/c1lc20020h. [PubMed: 21755093]

[11]. Jansen PGM, te Velthuis H, Bulder ER, Paulus R, Scheltinga MRM, Eijsman L, Wildevuur CRH, Reduction in prime volume attenuates the hyper-dynamic response after cardiopulmonary bypass, Ann. Thorac. Surg (1995) 10.1016/0003-4975(95)00385-X.

[12]. Cormack JE, Forest RJ, Groom RC, Morton J, Size makes a difference: use of a low-prime cardiopulmonary bypass circuit and autologous priming in small adults, Perfusion 15 (2000) 129–135 10.1177/026765910001500207. [PubMed: 10789567]

[13]. Anastasiadis K, Antonitsis P, Haidich AB, Argiriadou H, Deliopoulos A, Papakonstantinou C, Use of minimal extracorporeal circulation improves outcome after heart surgery; A systematic review and meta-analysis of randomized controlled trials, Int. J. Cardiol (2013) 10.1016/j.ijcard.2012.01.020.

[14]. Kovach KM, Labarbera MA, Moyer MC, Cmolik BL, Van Lunteren E, Sen Gupta A, Capadona JR, Potkay JA, In vitro evaluation and *in vivo* demonstration of a biomimetic, hemocompatible, microfluidic artificial lung, Lab Chip 15 (2015) 1366–1375 10.1039/C4LC01284D. [PubMed: 25591918]

[15]. Brisbois EJ, Handa H, Meyerhoff ME, Recent Advances in Hemocompatible Polymers for Biomedical Applications, Adv. Polym. Med (2015) 485–486 10.1007/978-3-319-12478-0.

[16]. Gokaltun A, Yarmush ML, Asatekin A, Usta OB, Recent advances in nonbio-fouling PDMS surface modification strategies applicable to microfluidic technology, TECHNOLOGY (2017) 10.1142/s2339547817300013.

[17]. Wo Y, Brisbois EJ, Bartlett RH, Meyerhoff ME, Recent advances in thromboresistant and antimicrobial polymers for biomedical applications: just say yes to nitric oxide (NO), Biomater. Sci (2016) 10.1039/c6bm00271d.

[18]. Seabra AB, Martins D, Simões MMSG, Da Silva R, Brocchi M, De Oliveira MG, Antibacterial nitric oxide-releasing polyester for the coating of blood-contacting artificial materials, Artif. Organs (2010) 10.1111/j.1525-1594.2010.00998.x.

[19]. Schoenfisch MH, Mowery KA, Rader MV, Baliga N, Wahr JA, Meyerhoff ME, Improving the thromboresistivity of chemical sensors via nitric oxide release: Fabrication and *in vivo* evaluation of NO-releasing oxygen-sensing catheters, Anal. Chem (2000) 10.1021/ac991370c.

[20]. Regev-Shoshani G, Ko M, Miller C, Av-Gay Y, Slow release of nitric oxide from charged catheters and its effect on biofilm formation by Escherichia coli, Antimicrob. Agents Chemother (2010) 10.1128/AAC.00511-09.

[21]. Reynolds MM, Frost MC, Meyerhoff ME, Nitric oxide-releasing hydrophobic polymers: Preparation, characterization, and potential biomedical applications, Free Radic. Biol. Med (2004) 10.1016/j.freeradbiomed.2004.06.019.

[22]. Zhou Z, Meyerhoff ME, Preparation and characterization of polymeric coatings with combined nitric oxide release and immobilized active heparin, Biomaterials (2005) 10.1016/j.biomaterials.2005.04.046.

[23]. Wu B, Gerlitz B, Grinnell BW, Meyerhoff ME, Polymeric coatings that mimic the endothelium: Combining nitric oxide release with surface-bound active thrombomodulin and heparin, Biomaterials (2007) 10.1016/j.biomaterials.2007.06.002.

[24]. Charville GW, Hetrick EM, Geer CB, Schoenfisch MH, Reduced bacterial adhesion to fibrinogen-coated substrates via nitric oxide release, Biomaterials (2008) 10.1016/j.biomaterials.2008.07.005.

[25]. Brisbois EJ, Major TC, Goudie MJ, Meyerhoff ME, Bartlett RH, Handa H, Attenuation of thrombosis and bacterial infection using dual function nitric oxide releasing central venous catheters in a 9-day rabbit model, Acta Biomater 44 (2016) 304–312 10.1016/j.actbio.2016.08.009. [PubMed: 27506125]

[26]. Ren H, Colletta A, Koley D, Wu J, Xi C, Major TC, Bartlett RH, Meyerhoff ME, Thromboresistant/anti-biofilm catheters via electrochemically modulated nitric oxide release, Bioelectrochemistry (2015) 10.1016/j.bioelechem.2014.12.003.

[27]. Mihu MR, Cabral V, Pattabhi R, Tar MT, Davies KP, Friedman AJ, Martinez LR, Nosanchuk JD, Sustained nitric oxide-releasing nanoparticles interfere with methicillinresistant staphylococcus aureus adhesion and biofilm formation in a rat central venous catheter model, Antimicrob. Agents Chemother (2017) 10.1128/AAC.02020-16.

[28]. Wo Y, Brisbois EJ, Wu J, Li Z, Major TC, Mohammed A, Wang X, Colletta A, Bull JL, Matzger AJ, Xi C, Bartlett RH, Meyerhoff ME, Reduction of Thrombosis and Bacterial Infection via Controlled Nitric Oxide (NO) Release from S-Nitroso-N-acetylpenicillamine (SNAP) Impregnated CarboSil Intravascular Catheters, ACS Biomater. Sci. Eng 3 (2017) 349–359 10.1021/acsbiomaterials.6b00622. [PubMed: 28317023]

[29]. Brisbois EJ, Kim M, Wang X, Mohammed A, Major TC, Wu J, Brownstein J, Xi C, Handa H, Bartlett RH, Meyerhoff ME, Improved Hemocompatibility of Multilumen Catheters via Nitric Oxide (NO) Release from S-Nitroso-N-acetylpenicillamine (SNAP) Composite Filled Lumen, ACS Appl. Mater. Interfaces 8 (2016) 29270–29279 10.1021/acsami.6b08707. [PubMed: 27734679]

[30]. Ren H, Coughlin MA, Major TC, Aiello S, Rojas Pena A, Bartlett RH, Meyerhoff ME, Improved *in vivo* Performance of Amperometric Oxygen (PO < inf>2 < /inf>) Sensing Catheters via Electrochemical Nitric Oxide Generation/Release, Anal. Chem (2015) 10.1021/acs.analchem.5b01590.

[31]. Kovach KM, Capadona JR, Sen Gupta A, Potkay JA, The effects of PEG-based surface modification of PDMS microchannels on long-term hemocompatibility, J. Biomed. Mater. Res. - Part A 102 (2014) 4195–4205 10.1002/jbm.a.35090.

[32]. Gimbel AA, Flores E, Koo A, García-Cardeña G, Borenstein JT, Development of a biomimetic microfluidic oxygen transfer device, Lab Chip 16 (2016) 3227–3234 10.1039/C6LC00641H. [PubMed: 27411972]

[33]. Rochow N, Manan A, Wu WI, Fusch G, Monkman S, Leung J, Chan E, Nagpal D, Predescu D, Brash J, Selvaganapathy PR, Fusch C, An Integrated Array of Microfluidic Oxygenators as a Neonatal Lung Assist Device: In Vitro Characterization and *In Vivo* Demonstration, Artif. Organs. 38 (2014) 856–866 10.1111/aor.12269. [PubMed: 24716531]

[34]. Plegue TJ, Kovach KM, Thompson AJ, Potkay JA, Stability of Polyethylene Glycol and Zwitterionic Surface Modifications in PDMS Microfluidic Flow Chambers, Langmuir 34 (2018) 492–502 10.1021/acs.langmuir.7b03095. [PubMed: 29231737]

[35]. Damodaran VB, Fee CJ, Popat KC, Prediction of protein interaction behaviour with PEG-grafted matrices using X-ray photoelectron spectroscopy, Appl. Surf. Sci (2010) 10.1016/j.apsusc.2010.02.088.

[36]. Kenworthy AK, Hristova K, Needham D, McIntosh TJ, Range and magnitude of the steric pressure between bilayers containing phospholipids with covalently attached poly(ethylene glycol), Biophys. J (1995) 10.1016/S0006-3495(95)80369-3.

[37]. Labouta HI, Gomez-Garcia MJ, Sarsons CD, Nguyen T, Kennard J, Ngo W, Terefe K, Iragorri N, Lai P, Rinker KD, Cramb DT, Surface-grafted polyethylene glycol conformation impacts the transport of PEG-functionalized liposomes through a tumour extracellular matrix model, RSC Adv (2018) 10.1039/c7ra13438j.

[38]. Tao SL, Popat KC, Norman JJ, Desai TA, Surface modification of SU-8 for enhanced biofunctionality and nonfouling properties, Langmuir (2008) 10.1021/la703066z.

[39]. Damodaran VB, Fee CJ, Popat KC, Modeling of PEG grafting and prediction of interfacial force profile using x-ray photoelectron spectroscopy, Surf. Interface Anal (2012) 10.1002/sia.3783.

[40]. Murat M, Grest GS, Structure of a Grafted Polymer Brush: A Molecular Dynamics Simulation, Macromolecules (1989) 10.1021/ma00200a041.

[41]. Ham AS, Klibanov AL, Lawrence MB, Action at a distance: Lengthening adhesion bonds with Poly(ethylene glycol) spacers enhances mechanically stressed affinity for improved vascular targeting of microparticles, Langmuir (2009) 10.1021/la900966h.

[42]. Onyskiw PJ, Eniola-Adefeso O, Effect of PE gylation on ligand-based targeting of drug carriers to the vascular wall in blood flow, Langmuir (2013) 10.1021/la402182j.

[43]. Bates JN, Nitric oxide measurement by chemiluminescence detection, Neuroprotocols (1992) 10.1016/1058-6741(92)90045-Y.

[44]. Burgess KA, Hu HH, Wagner WR, Federspiel WJ, Towards microfabricated biohybrid artificial lung modules for chronic respiratory support, Biomed. Microdevices 11 (2009) 117–127 10.1007/s10544-008-9215-2. [PubMed: 18696229]

[45]. Wu WI, Rochow N, Chan E, Fusch G, Manan A, Nagpal D, Selvaganapathy PR, Fusch C, Lung assist device: development of microfluidic oxygenators for preterm infants with respiratory failure, Lab Chip 13 (2013) 2641–2650 10.1039/c3lc41417e. [PubMed: 23702615]

[46]. Thompson A, Marks L, Goudie M, Rojas-Pena A, Handa H, Potkay J, A small-scale, rolled-membrane microfluidic artificial lung designed towards future large area manufacturing., Biomicrofluidics (2017) 11.

[47]. Rochow N, Wu WI, Chan E, Nagpal D, Fusch G, Selvaganapathy PR, Monkman S, Fusch C, Integrated microfluidic oxygenator bundles for blood gas exchange in premature infants, in: Proc. IEEE Int. Conf. Micro Electro Mech. Syst., 2012, pp. 957–960. 10.1109/MEMSYS.2012.6170345.

[48]. Malankowska M, Julian I, Pellejero I, Rho HS, Schlautmann S, Tiggelaar RM, Pina MP, Gardeniers HJGE, Mallada R, Understanding blood oxygenation in a microfluidic meander double side membrane contactor, Sensors Actuators, B Chem (2019) 10.1016/j.snb.2019.02.110.

[49]. Kniazeva T, Hsiao JC, Charest JL, Borenstein JT, A microfluidic respiratory assist device with high gas permeance for artificial lung applications, Biomed. Microdevices 13 (2011) 315–323 10.1007/s10544-010-9495-1. [PubMed: 21113664]

[50]. Kniazeva T, Epshteyn AA, Hsiao JC, Kim ES, Kolachalama VB, Charest JL, Borenstein JT, Performance and scaling effects in a multilayer microfluidic extracorporeal lung oxygenation device, Lab Chip 12 (2012) 1686–1695 10.1039/c2lc21156d. [PubMed: 22418858]

[51]. Hoganson DM, Anderson JL, Weinberg EF, Swart EJ, Orrick BK, Borenstein JT, Vacanti JP, Branched vascular network architecture: A new approach to lung assist device technology, J. Thorac. Cardiovasc. Surg (2010) 10.1016/j.jtcvs.2010.02.062.

[52]. Dabaghi M, Fusch G, Saraei N, Rochow N, Brash JL, Fusch C, Ravi Selvaganapathy P, An artificial placenta type microfluidic blood oxygenator with double-sided gas transfer microchannels and its integration as a neonatal lung assist device, Biomicrofluidics (2018) 10.1063/1.5034791.

[53]. Vollmer AP, Snyder TA, Kamaneva MV, Monzyk BF, Burckle EC, Dasse KA, Martin PM, Borovetz HS, Wagner WR, Gilbert RJ, Thorsen TA, DEVELOPMENT OF A 2D MICROFLUIDIC OXYGENATION DEVICE, ASAIO J. Artif. Organ Res. Dev (2005) 51 https://journals.lww.com/asaiojournal/Fulltext/2005/03000/DEVELOPMENT_OF_A_2D_MICROFLUIDIC_OXYGENATION.210.aspx.

[54]. Gilbert RJ, Park H, Rasponi M, Redaelli A, Gellman B, Dasse KA, Thorsen T, Computational and functional evaluation of a microfluidic blood flow device, ASAIO J (2007) 10.1097/MAT.0b013e3180a5e8ab.

[55]. Passarella RJ, Spratt DE, Van Der Ende AE, Phillips JG, Wu H, Sathiyakumar V, Zhou L, Hallahan DE, Harth E, Diaz R, Targeted nanoparticles that deliver a sustained, specific release of paclitaxel to irradiated tumors, Cancer Res 70 (2010) 4550–4559 10.1158/0008-5472.CAN-10-0339. [PubMed: 20484031]

[56]. Borenstein JT, Terai H, King KR, Weinberg EJ, Kaazempur-Mofrad MR, Vacanti JP, Microfabrication technology for vascularized tissue engineering, Biomed. Microdevices 4 (2002) 167–175 10.1023/A:1016040212127.

[57]. Burgess KA, Hu HH, Wagner WR, Federspiel WJ, Towards microfabricated biohybrid artificial lung modules for chronic respiratory support, Biomed. Microdevices (2009) 10.1007/s10544-008-9215-2.

[58]. Zhang Z, Borenstein J, Guiney L, Miller R, Sukavaneshvar S, Loose C, Polybetaine modification of PDMS microfluidic devices to resist thrombus formation in whole blood, Lab Chip 13 (2013) 1963 10.1039/c3lc50302j. [PubMed: 23563730]

[59]. Amoako KA, Montoya PJ, Major TC, Suhaib AB, Handa H, Brant DO, Meyerhoff ME, Bartlett RH, Cook KE, Fabrication and *in vivo* thrombogenicity testing of nitric oxide generating artificial lungs, J. Biomed. Mater. Res. - Part A (2013) 10.1002/jbm.a.34655.

[60]. Lai A, Demarest CT, Do-Nguyen CC, Ukita R, Skoog DJ, Carleton NM, Amoako KA, Montoya PJ, Cook KE, 72-Hour *in vivo* evaluation of nitric oxide generating artificial lung gas exchange fibers in sheep, Acta Biomater (2019) 10.1016/j.actbio.2019.04.004.

[61]. Amoako KA, Sundaram HS, Suhaib A, Jiang S, Cook KE, Multimodal, Biomaterial-Focused Anticoagulation via Superlow Fouling Zwitterionic Functional Groups Coupled with Anti-Platelet Nitric Oxide Release, Adv. Mater. Interfaces 3 (2016) n/a–n/a 10.1002/admi.201500646.

[62]. Gupta S, Amoako KA, Suhaib A, Cook KE, Multi-Modal, Surface-Focused Anticoagulation Using Poly-2-methoxyethylacrylate Polymer Grafts and Surface Nitric Oxide Release, Adv. Mater. Interfaces (2014) 10.1002/admi.201400012.

[63]. Wright RO, Lewander WJ, Woolf AD, Methemoglobinemia: Etiology, pharmacology, and clinical management, Ann. Emerg. Med (1999) 10.1016/S0196-0644(99)70167-8.

[64]. Mansouri A, Lurie AA, Methemoglobinemia, Am. J. Hematol (1993) 10.1002/ajh.2830420104.

[65]. Vaughn MW, Estimation of nitric oxide production and reaction rates in tissue by use of a mathematical model, Am. J. Physiol. Heart Circ. Physiol 274 (1998) H2163–H2176.

[66]. Goudie MJ, Brisbois EJ, Pant J, Thompson A, Potkay JA, Handa H, Characterization of an S-nitroso-N-acetylpenicillamine–based nitric oxide releasing polymer from a translational perspective, Int. J. Polym. Mater. Polym. Biomater (2016) 65 10.1080/00914037.2016.1163570.

[67]. Lee S, Vörös J, An aqueous-based surface modification of poly(dimethylsiloxane) with poly(ethylene glycol) to prevent biofouling, Langmuir (2005) 10.1021/la051932p.

Statement of significance

The development of microfluidic artificial lungs (μALs) can potentially have a massive impact on the treatment of patients with acute and chronic lung impairments. Before these devices can be deployed clinically, the biocompatibility of μALs must be improved and more comprehensively understood. This work explores two strategies for improving biocompatibility, a hydrophilic surface coating (polyethylene glycol) for general surface passivation and the addition of nitric oxide (NO) to the sweep gas to quell platelet and leukocyte activation. These two strategies are investigated separately and as a combined device treatment. Devices are challenged with clottable blood using *in vitro* testing and *in vivo* testing in rabbits. This is the first study to our knowledge that allows statistical comparisons of biocompatible μALs in animals, a key step towards eventual clinical use.

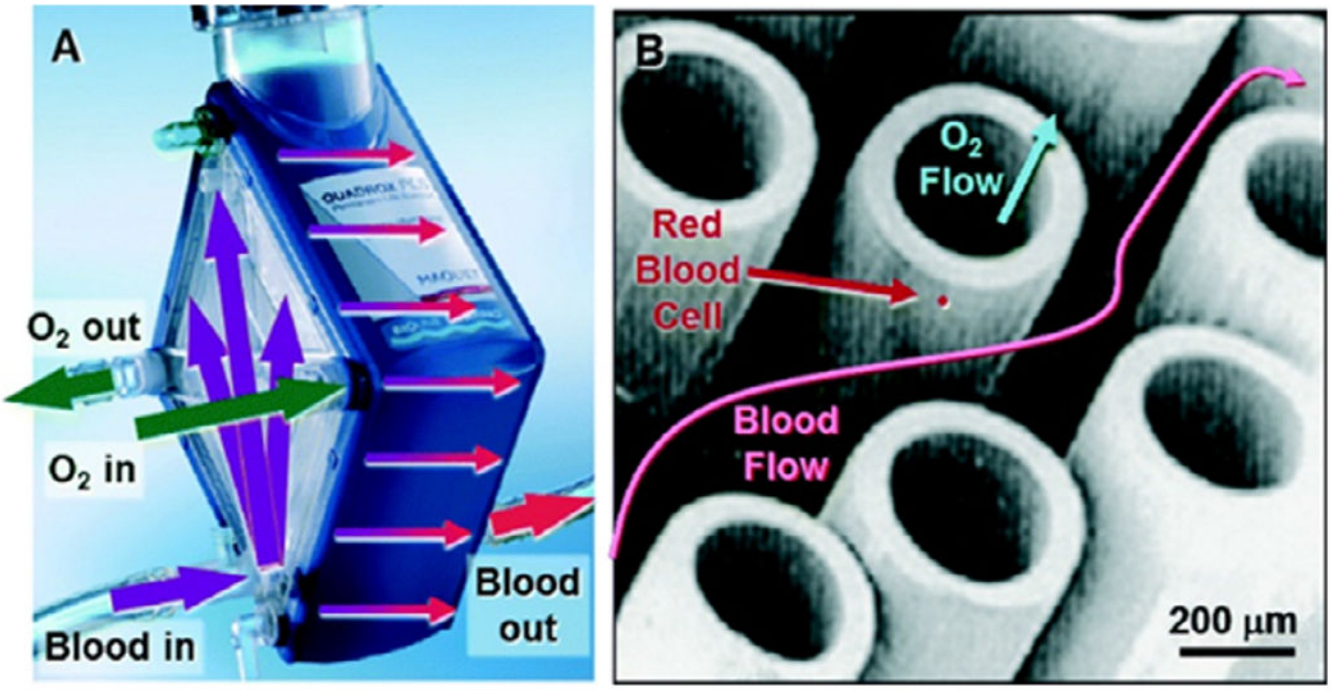

Fig. 1.

(A) Maquet Quadrox-PLSi oxygenator with arrows indicating the general flow path for blood and sweep gas. (B) Representative image of membrane fibers used in clinical oxygenators. Reproduced from Potkay JA, Lab on a Chip (2014) with permission from Royal Society of Chemistry.

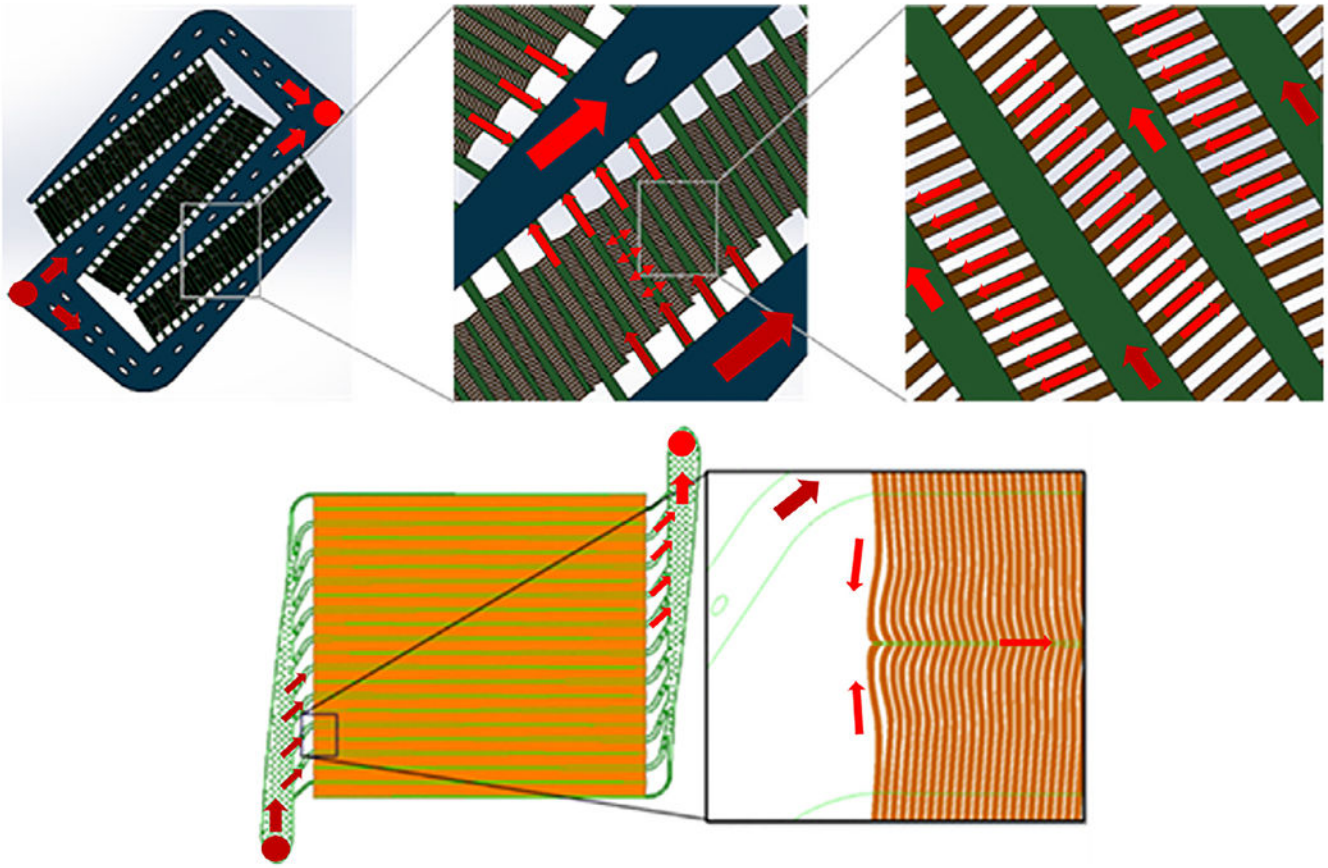

Fig. 2.

2D Schematics of the blood flow network for μALs used for *in vitro* (top) and *in vivo* (bottom) studies. Devices used for *in vitro* studies had a branching distribution network consisting of 180 μm (blue) and 60 μm (green) channel heights, and artificial capillaries with 12 μm channel height (brown, top right image). Devices used for *in vivo* studies had a branching distribution network consisting of 250 μm channel heights (green) and 30 μm tall capillaries (orange). A full description of the design used for *in vivo* studies can be found in the cited work. [8]

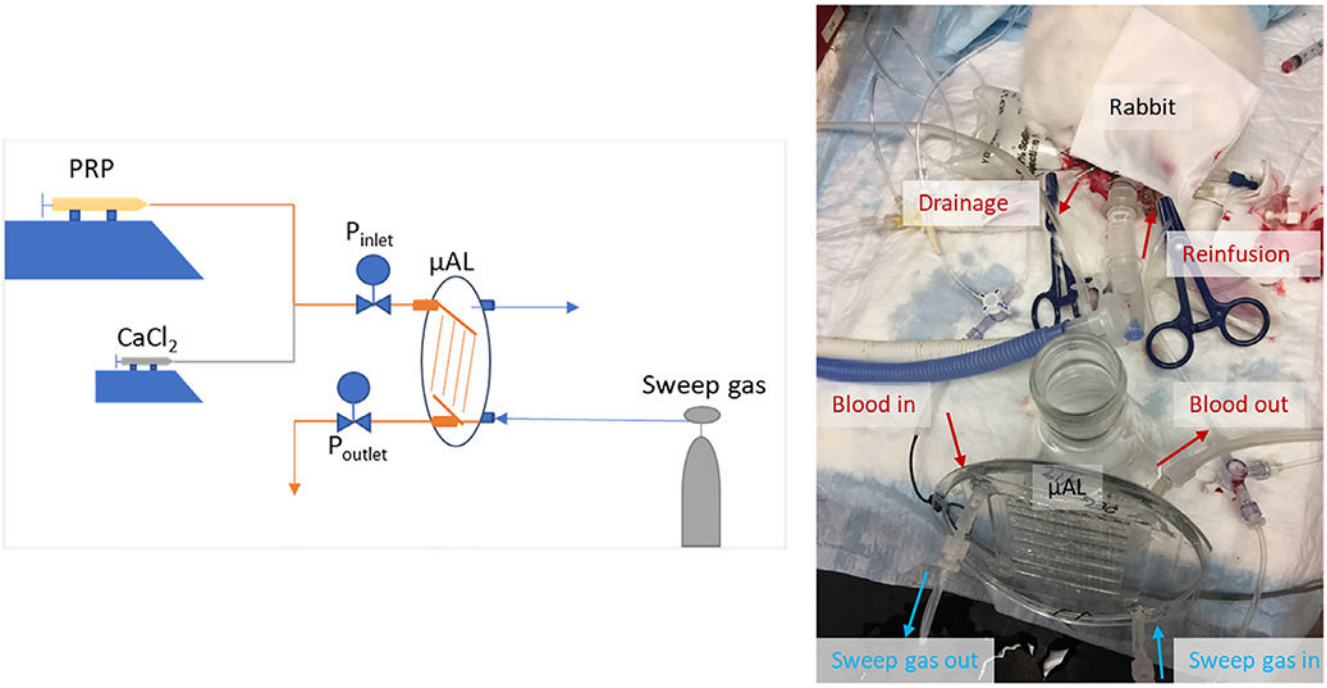

Fig. 3.

Schematic of in vitro hemocompatibiiity test setup (left) and a representative AV µAL circuit used for *in vivo* biocompatibility testing (right).

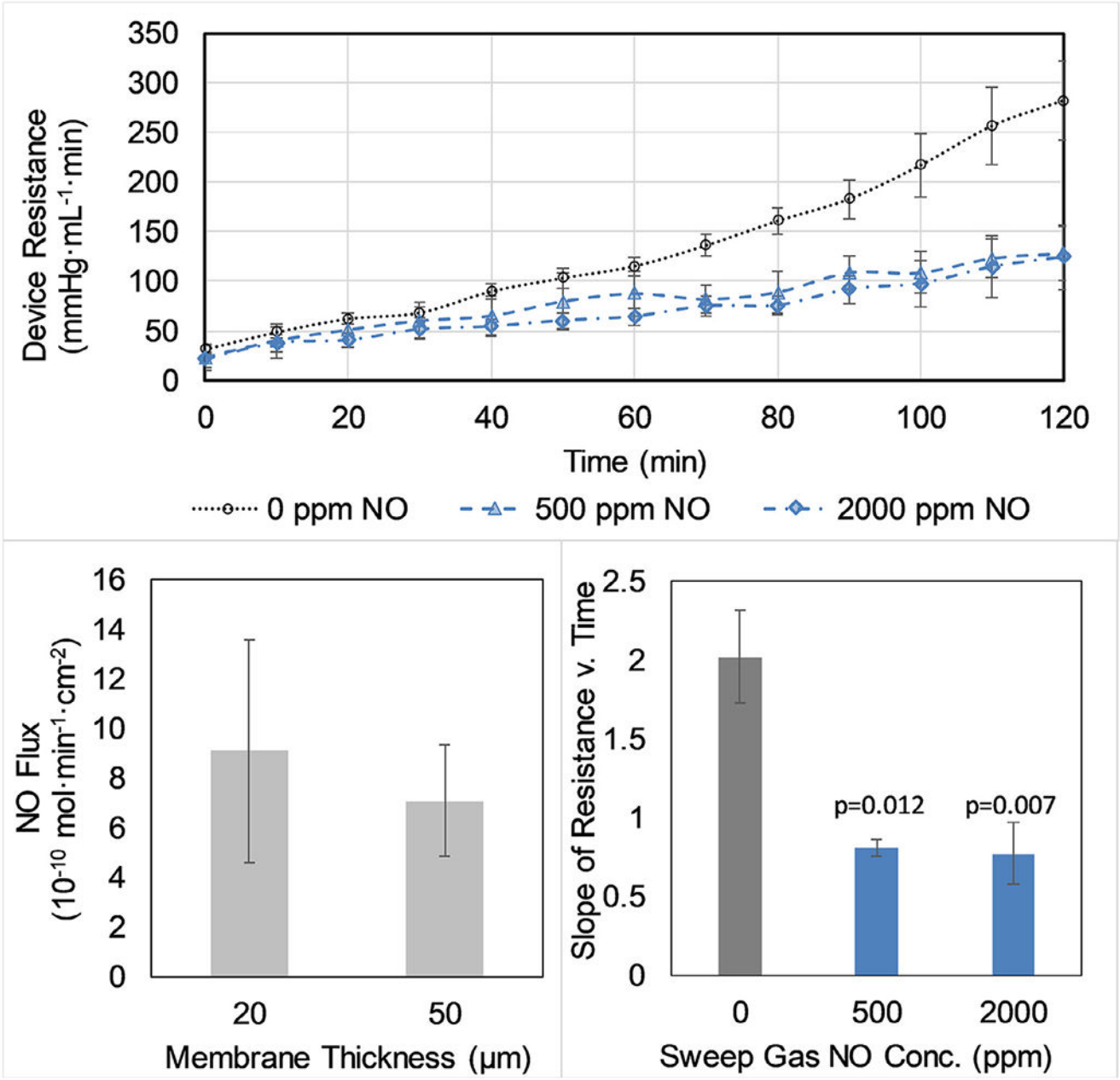

Fig. 4.

Resistance to flow of bovine PRP in small-scale μALs during two-hour in vitro flow testing (top). Devices received either inert N2 sweep gas or NO sweep gas (either 500 ppm or 2000 ppm NO in N2). The rate of increasing flow resistance with time (mmHg mL^{-1}, estimated via linear regression of the experimental data) is significantly lower in both NO sweep gas groups compared to the control group (bottom right). NO-doped sweep gas results in a measurable flux of NO across the membrane of the μAL when tested with saline and 2000 ppm NO sweep gas (bottom left).

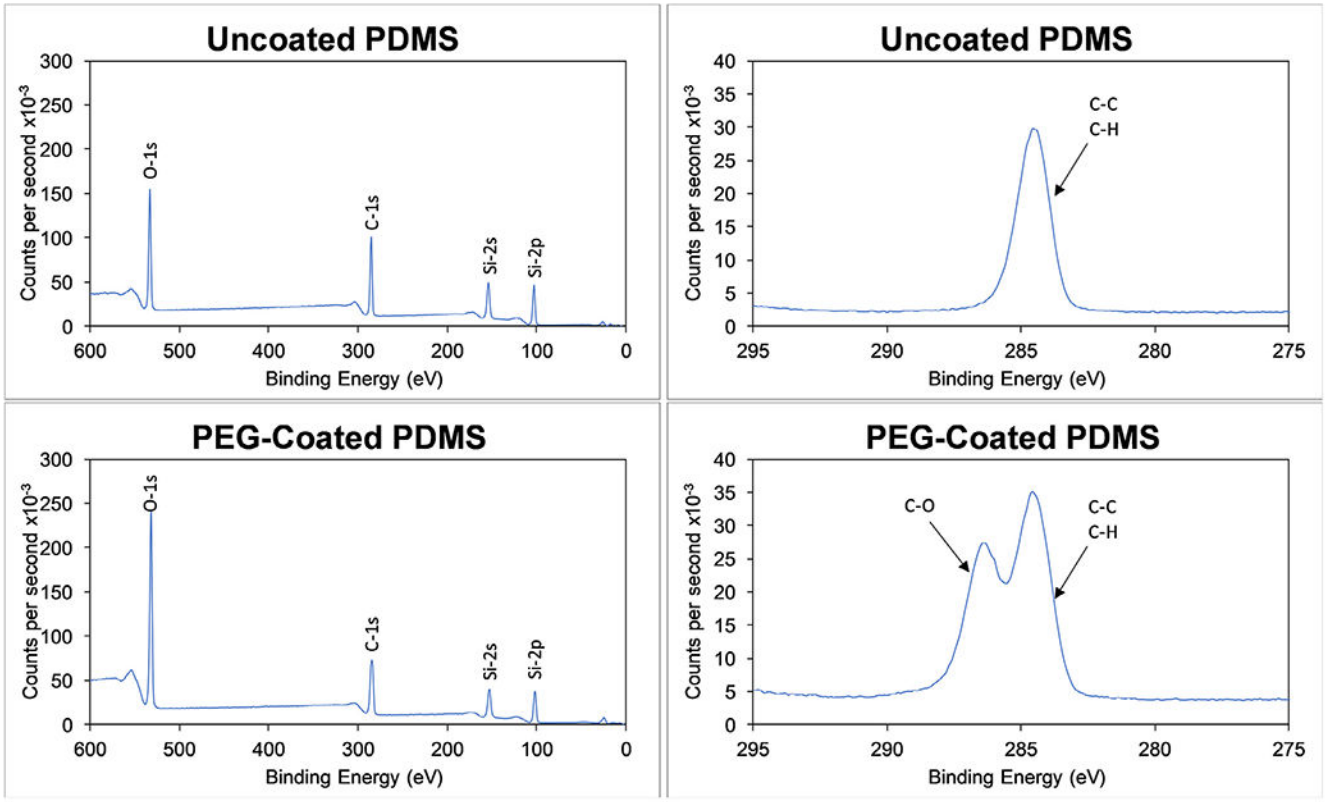

Fig. 5.

Survey scans (left) and high-resolution C-1s scans (right) of uncoated PDMS (top) and PEG-coated PDMS (bottom) surfaces analyzed using XPS.

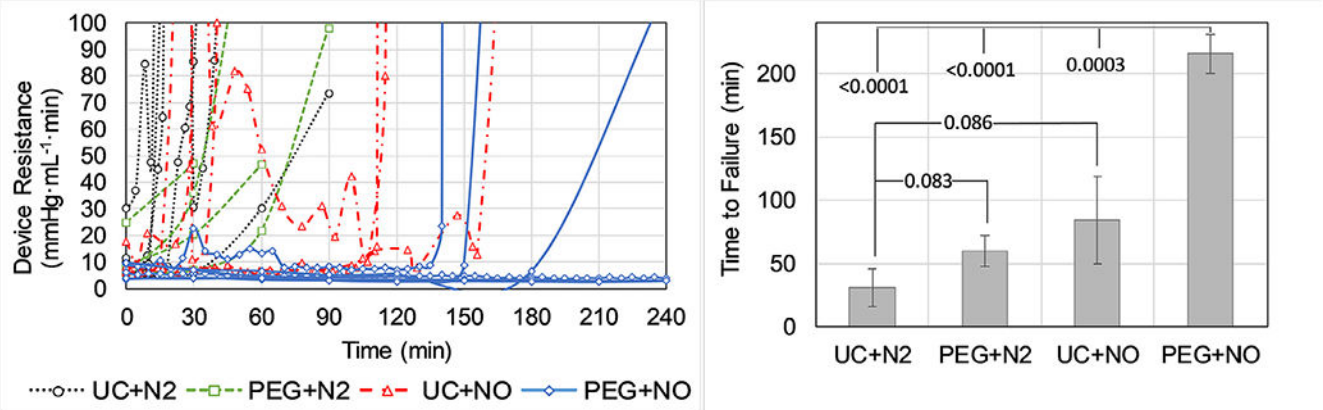

Fig. 6.

Blood flow resistance in μALs used in a pumpless arteriovenous circuit in rabbits for 4 hours. Devices were either uncoated (UC) or PEG-coated (PEG) and received either nitrogen (N2) or 1000 ppm NO (NO) sweep gas. Individual trials (left) were run until device flow stopped due to clotting or at 4 hours and the time to failure for each group was averaged (right).

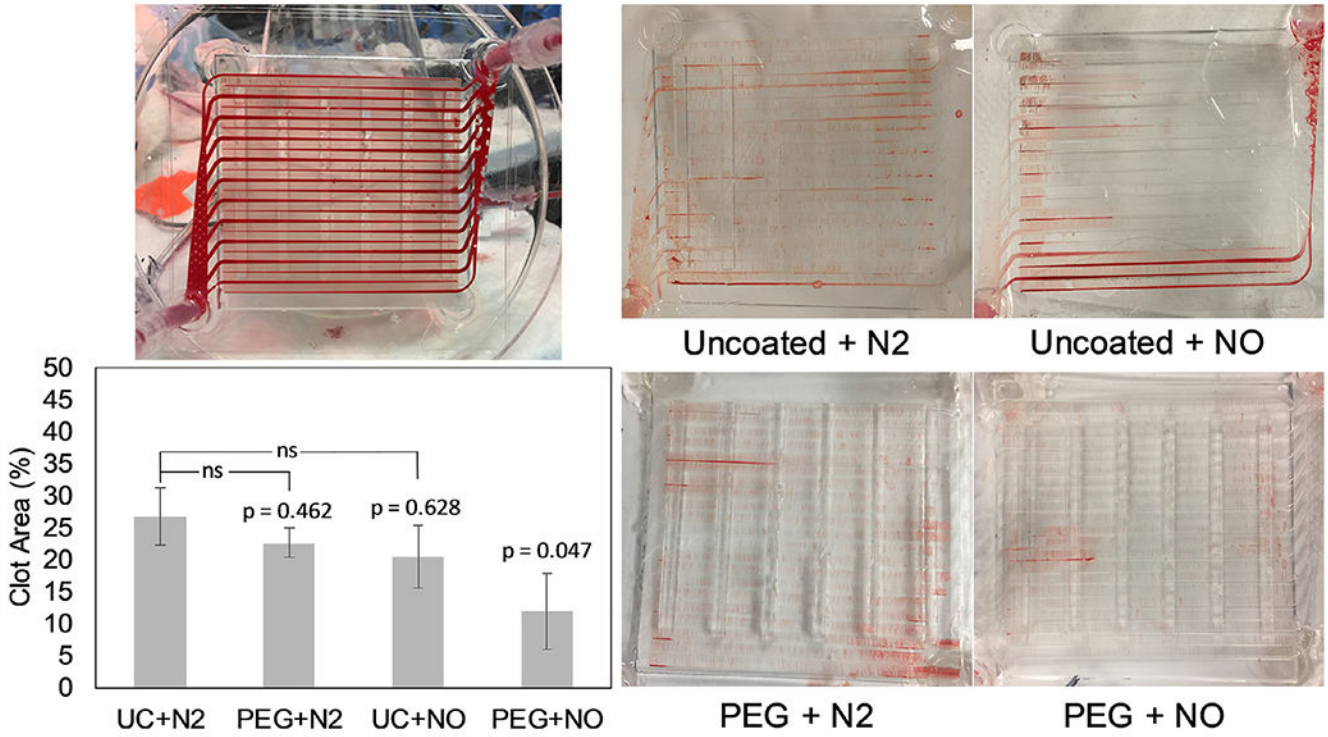

Fig. 7.

Residual clot area in μALs following *in vivo* rabbit AV circuit tests. Devices were either uncoated (UC) or PEG-coated (PEG) and received either nitrogen (N2) or 1000 ppm NO (NO) sweep gas. Representative images are shown of a device facilitating active blood flow during an *in vivo* test (top left), and of devices from each group following the post-experiment saline flush (right). P-values are shown for comparisons to the UC+N2 group. ns = not significant, $p>0.05$.

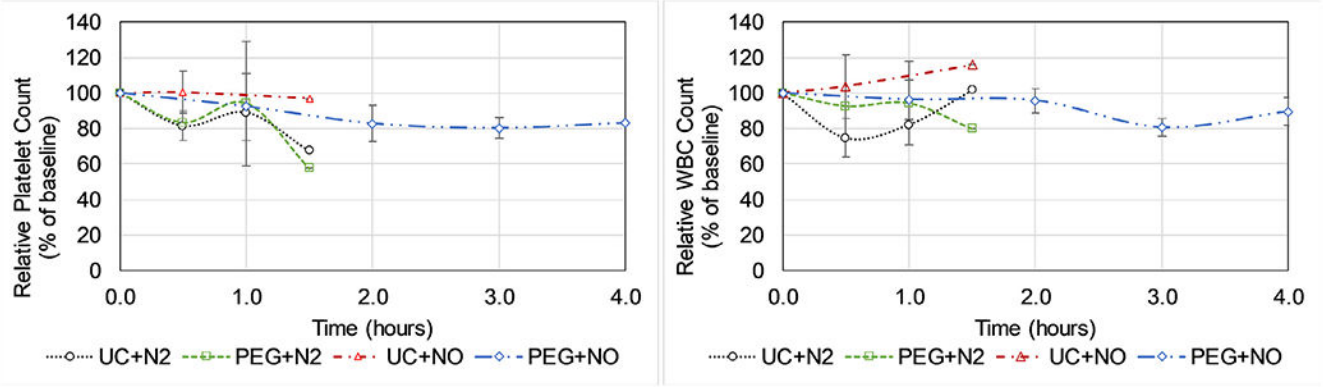

Fig. 8.

Platelet (left) and leukocyte (right) counts during *in vivo* μAL testing. Datapoints without error bars only had data from 1 trial due to device failure prior to that timepoint in the other trials. Devices were either uncoated (UC) or PEG-coated (PEG) and received nitrogen (N2) or 1000 ppm NO (NO) sweep gas. The baseline blood data was obtained once the surgical cannulations have been completed and once the ACT is confirmed to be within the desired range, but prior to opening blood flow through the device and extracorporeal tubing.